Novel Low-Pass Filter Structures Using Spur-Lines to Generate Additional Attenuation Poles

In-seon Kim[1]*, Beom-Jun Park[2], Cheol-Soo Lee[3], Joo-Rae Park[4] and Ghi-Back Kim[5]

[1,2,3,4,5] *Agency for Defense Development, P.O. Box35, Yuseong, Daejeon, 34186, Korea*

*Correspondence: In-seon Kim; naechon199@naver.com; Tel.: +82-42-821-3545

ABSTRACT- We propose two novel low-pass filter (LPF) structures that have generated additional attenuation poles from applying spur-lines to typical open-stub LPFs. The first structure has the spur-lines added to the serial lines, and the second structure has the spur-lines added to the parallel open stub. From the characteristic analyses of the filters with the proposed design, it was confirmed that the length of the spur-line was an important variable for controlling the stopband bandwidth and attenuation depth. The two types of LPFs were fabricated and then validated by the agreement between the theoretical and measured results. From the measured results, the stopband bandwidths of the serial- and parallel-configuration spur-line LPFs were improved by approximately 4.7 times and 1.4 times of the defined reference level, respectively, compared to that of the typical LPF.

Keywords: Spur-line, equivalent circuit, attenuation pole, stopband bandwidth.

Publisher's Note: FOREX Publication stays neutral with regard to Jurisdictional claims in Published maps and institutional affiliations.

1. INTRODUCTION

Low-pass filters (LPFs) are widely employed to suppress harmonics and spurious signals in communication systems. The performance of an LPF is defined by the characteristics of its skirt, passband insertion loss, and stopband attenuation. Therefore, incorporating measures to ensure excellent performance is the main goal of LPF design, which can be achieved by various methods. Among these, microstrip open-stub LPFs (OSLPF) and stepped-impedance line LPFs are the most widely used types because of their ease of design and manufacturing. However, these structures generate harmonics and spurious responses based on the periodicity of the transmission-line length; this is one of the main reasons for limiting wide stopband implementation. Therefore, many studies have been conducted on suppression of unwanted signals, such as harmonics and spurious responses; LPF structures using a ground plane, such as PBG and DGS [1-4], and structures using coupled lines [5-7] are representative examples of such studies. In addition, several other studies have been conducted on various structures to generate additional attenuation poles in the stopband [8-11]. In this study, to improve the stopband performance, we consider two novel structures of the LPF using spur-lines; the configurations of the two proposed LPFs are modified from the basic structure of the OSLPF. The first structure has the spur-line added to the serial lines of the OSLPF, and the second structure has the spur-line added to the parallel stub. We named the first configuration as serial spur-line LPF (SSLPF) and the second as parallel spur-line LPF (PSLPF). The equivalent structures for these two LPFs are presented, and the required design formulas are derived. Then, the two types of LPFs were fabricated and validated by theoretical analysis as well as the simulated and measured results

2. SYNTHESIS OF THE SSLPF

The first proposed structure is the SSLPF, where the spur-line is added to the serial transmission line of the typical OSLPF structure. This structure allows improved stopband characteristics by generating additional attenuation poles in the stopband while maintaining the passband characteristics of the OSLPF using the spur-lines. *Figure 1(a)* depicts the typical structure of the OSLPF, and *figure 1(b)* shows the proposed SSLPF.
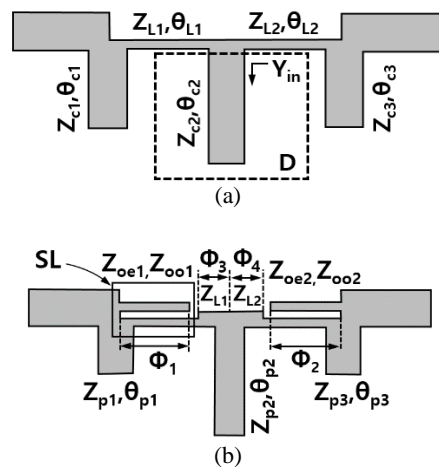

Figure 1. (a) Typical OSLPF structure; (b) Proposed SSLPF structure

In *figure 1(b)*, the box SL depicts the spur-line unit structure;

further, Φ_3 and Φ_4 are equal to θ_{L1}-Φ_1 and θ_{L2}- Φ_2, respectively. The spur-line can be represented by the equivalent circuit shown in *figure 2* [12-13].

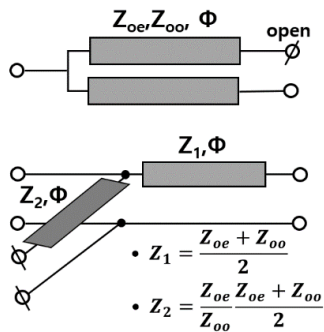Figure 2.Equivalent structure of the spur-line (SL) in *figure 1(b)*

If the spur-line structure of *figure 2* were to be applied to the serial line of *figure 1(a)*, then the equivalent structure can be expressed as *figure 3(a)*, where X-X′ is the axis of symmetry. Therefore, the variables corresponding to the left and right sides about this axis are identical, and only the variables on left side of the central axis will be described from this point forward.
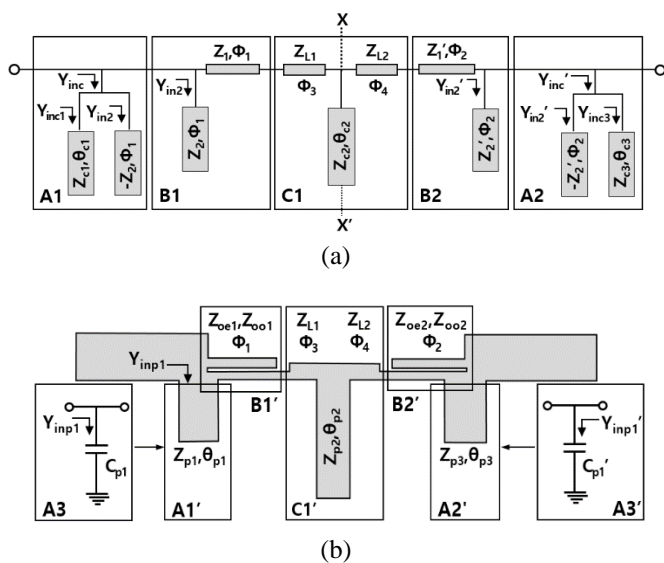

Figure 3. (a) Structure with spur-line equivalent applied to the OSLPF; (b) changes Structural to the OSLPF to obtain the SSLPF

Boxes A1, B1, and C1 in *figure 3(a)* correspond to boxes A1′, B1′, and C1′ in *figure 3(b)*, respectively. Thus, when all the parts are matched, the structure in *figure 1(a)* is transformed to that in *figure 1(b)*. In *figure 3(a)*, the spur-line impedance is defined as the impedance (Z_{L1}) of the serial line to simplify the calculation and minimize the discontinuity of the serial transmission line; the length Φ_1 is set to $\lambda/4$ at the desired frequency such that the attenuation pole can be generated at that frequency. Y_{inc} in *figure 3(a)* is calculated as shown in *equation (1)*.

$$Y_{inc} = Y_{inc1} + Y_{in2}$$
$$= j\left[Y_{c1}tan\theta_{c1} - \frac{Z_{oe1}}{Z_{oo1}}\left(\frac{Z_{oo1}+Z_{oe1}}{2}\right)tan\emptyset_1\right] \quad (1)$$

Here, Y_{in2} is obtained using Z_2 in *figure 2*.

The equivalent capacitance can be calculated using *equation (2)* under the condition that A1 and A3 are identical.

$$Y_{inc} = j\omega_c C_{p1}$$
$$C_{p1} = \frac{1}{\omega_c}\left[Y_{c1}\tan\theta_{c1} - \frac{Z_{oe1}}{Z_{oo1}}\left(\frac{Z_{oo1}+Z_{oe1}}{2}\right)tan\emptyset_1\right] \quad (2)$$

Using the C_{p1} calculated with *equation (2)* and the required open-stub impedance, the modified length of the outermost open stub can be obtained as shown in *equation (3)*.

$$Y_{p1}tan\theta_{p1} = \omega_c C_{p1}$$
$$\theta_{p1} = tan^{-1}\left(Z_{p1}\left[Y_{c1}tan\theta_{c1} - \frac{Z_{oe1}}{Z_{oo1}}\left(\frac{Z_{oo1}+Z_{oe1}}{2}\right)tan\emptyset_1\right]\right) \quad (3)$$

As shown in *figure 3*, only the outermost open stubs are affected by the spur-lines but that in the middle is not affected; this means that in *figures 1(a) and 1(b)*, Z_{c2} is Z_{p2} and θ_{c2} is θ_{p2}.

Figure 4 shows the characteristics of the SSLPFs with $f_c = 2$ GHz for several spur-line lengths. The design parameters for simulating the OSLPF as shown in figure 1(a) are $Z_{c1} = 50$ Ω, $Z_{L1} = 80$ Ω, $Z_{c2} = 50$ Ω, $\theta_{c1} = 23.62$, $\theta_{L1} = 54.28°$, and $\theta_{c2} = 43.21°$. Meanwhile, the design parameters of the SSLPF as shown in *figure 1(b)* are $Z_{oe1} = 88$ Ω, $Z_{oo1} = 72.73$ Ω, and $\theta_{p2} = 43.21°$. θ_{p1} and Φ_3 are variables that are changed by Φ_1
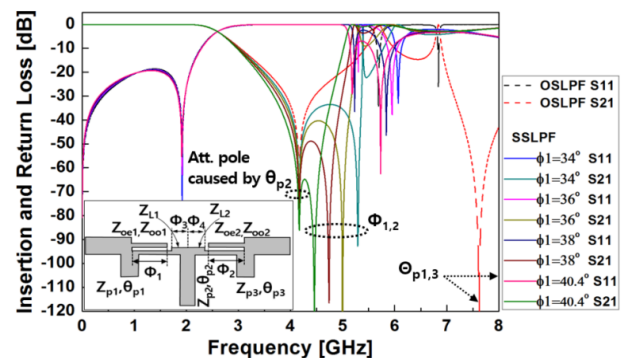

Figure 4. Characteristics of the SSLPF based on spur-line length

Figure 4 shows that when the length of the spur-line is changed, the passband characteristics remain similar to those of the OSLPF; however, it can be seen that the position of the attenuation pole changes according to the length of the spur-line (Φ_1), and θ_{p2} is not affected by Φ_1. Therefore, we see that the first attenuation poles are formed equally at the frequency where θ_{p2} is equal to $\lambda/4$ in all cases. The second attenuation poles are formed at the frequency where the length of the spur-line is $\lambda/4$. Accordingly, if the length of the spur-line is set correctly, the positions of the second attenuation poles can be adjusted with reference to the fixed first attenuation poles such that the stopband bandwidth and attenuation depth can be controlled partially. One of the notable features of this structure is that θ_{p1} can be calculated as zero if Φ_1 is selected appropriately; this means that the open stub can be removed if needed.

3. SYNTHESIS OF THE PSLPF

The second proposed structure is the PSLPF, where the spur-line is added to the parallel open stub of the typical OSLPF structure, as depicted in *figure 5*.
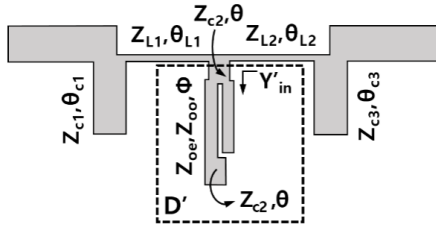

Figure 5. Proposed PSLPF structure

If the dotted box *D* in *figure 1(a)* is equivalent to the dotted box *D′* in *figure 5*, then the passband characteristics of the LPF are the same. However, the structure in *figure 5* can generate additional attenuation poles in the stopband compared to that in *figure 1(a)*. *Figure 6* shows the equivalent structure of the dotted box *D′* from *figure 5*.
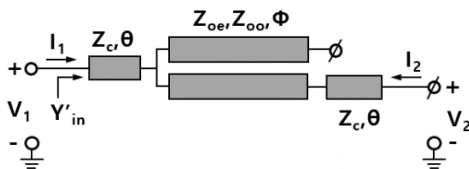

Figure 6. Equivalent structure of the box D′ in *figure 5*

In *figure 6*, Y_{in}' is calculated using *equation (4)* with the ABCD parameters and termination condition with I_2 equal to zero.

$$Y_{in}' = j\frac{\delta \cdot tan\theta - \gamma \cdot tan^2\theta + 4sin\theta}{2Z_{oe}cos\emptyset - \alpha \cdot tan\theta + \beta \cdot tan^2\theta} \tag{4}$$

Here, α, β, δ, and γ are as follows:

$$\alpha = [4Z_c + Y_c Z_{oe}(Z_{oe} + Z_{oo})]sin\theta$$

$$\beta = 2(Z_{oe}sin\emptyset \cdot tan\emptyset - Z_{oo}cos\emptyset)$$

$$\delta = 4Y_c Z_{oe}cos\emptyset - 2Y_c Z_{oo}Z_{oe}sin\emptyset \cdot tan\emptyset$$

$$\gamma = Y_c^2 Z_{oe}(Z_{oe} + Z_{oo})sin\emptyset$$

The input admittance of the dotted box *D* in *figure 1(a)* is as shown in *equation (5)*.

$$Y_{in} = jY_{c2}tan\theta_{c2} \tag{5}$$

Further, if Y_{in} and Y_{in}' are the same in *equation (6)*, then dotted boxes *D* in *figure 1(a)* and *D′* in *figure 5* are equivalent structures.

$$j\frac{\delta \cdot tan\theta - \gamma \cdot tan^2\theta + 4sin\theta}{2Z_{oe}cos\emptyset - \alpha \cdot tan\theta + \beta \cdot tan^2\theta} = jY_{c2}tan\theta_{c2} \tag{6}$$

Equation (6) can be expressed as a polynomial of tanθ, as shown in *equation (7)*.

$$C_1 tan^2\theta - C_2 tan\theta + C_3 = 0 \tag{7}$$

Here, the coefficients C_1, C_2, and C_3 are as follows:

$$C_1 = \beta Y_{c2}tan\theta_{c2} + \gamma$$

$$C_2 = \alpha Y_{c2}tan\theta_{c2} + \delta$$

$$C_3 = 2Y_{c2}Z_{oe}tan\theta_{c2}cos\emptyset - 4sin\emptyset$$

From the solution of *equation (7)*, we can obtain θ as in *equation (8)*.

$$\theta = \frac{C_2 - \sqrt{C_2^2 - 4C_1 C_3}}{2C_1} \tag{8}$$

Figure 7 shows the characteristics of the PSLPFs with $f_c = 2$ GHz for several spur -line lengths. The design parameters for simulating the OSLPF are $Z_{c1} = 40 \ \Omega$, $Z_{L1} = 100 \ \Omega$, $Z_{c2} = 40 \ \Omega$, $\theta_{c1} = 24.54$, $\theta_{L1} = 40.73°$, and $\theta_{c2} = 24.54$. Meanwhile, the design parameters of the PSLPF are $Z_c = 40 \ \Omega$, $Z_{oe} = 45 \ \Omega$ and, $Z_{oo} = 35.56 \ \Omega$; θ is a variable that is changed by Φ. The other parameters (Z_{c1}, Z_{L1}, θ_{c1}, and θ_{L1}) are identical to those of the OSLPF.
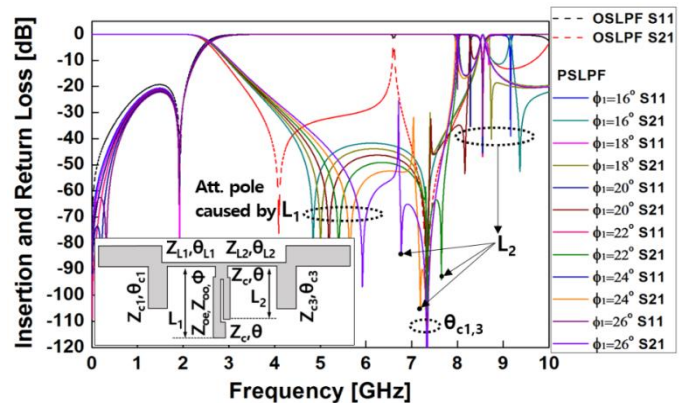

Figure 7. Characteristics of the PSLPF based on spur-line length

From *figure 7*, it can be seen that when the length of the spur-line is changed, the passband characteristics remain identical to those of the OSLPF. The attenuation poles generated by θc1 and θc3, which are not affected by the spur-line, are formed at the same frequency; this means that the second attenuation poles in all cases are formed equally at the frequency where θc1 and θc3 are equal to λ/4. The first and third attenuation poles are generated by L1 and L2, which are affected by the length (Φ) of the spur-line. Similar to the case of the SSLPF, the stopband bandwidth and attenuation depth of the PSLPF can be adjusted according to the distribution of the attenuation poles.

4. FABRICATION OF THE FILTERS AND ANALYSIS OF THE RESULTS

To validate the proposed structures and derived equations, the SSLPF and PSLPF were designed and fabricated. Simulations were performed using the CST Microwave Studio. A substrate

with H = 0.7874 mm and ε_r = 2.2 were used for the simulation and fabrication.

4.1 Fabrication and Evaluation of the SSLPF

This LPF was designed as a Chebyshev filter with fc = 2 GHz, N=5, and passband ripple of 0.01 db. The design parameters of the transmission lines for manufacturing were set as Zoe1 = 88 Ω, Zoo1 = 72.73 Ω, ZL1 = 80 Ω, Zp2 = 50 Ω, Φ1= 40.39°, Φ3= 13.79°, and θp2 = 43.21°. Meanwhile, θp1 was calculated using *equation (3)* as zero; this means that the first and third open stubs have been removed. *Figure 8* presents a photograph of the fabricated SSLPF.
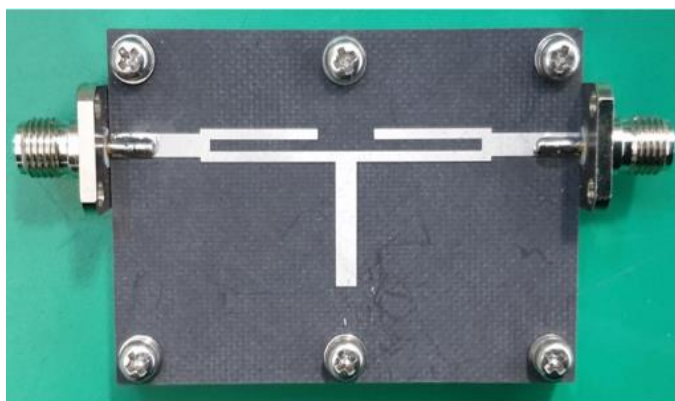

Figure 8. Fabricated SSLPF

In the SSLPF shown in *figure 8*, we see that the outermost open stubs have been removed, as originally designed. *Figure 9* shows the electromagnetic (EM) simulated and measured results of the fabricated SSLPF; the typical OSLPF characteristics are also presented to show the improved stopband performance.
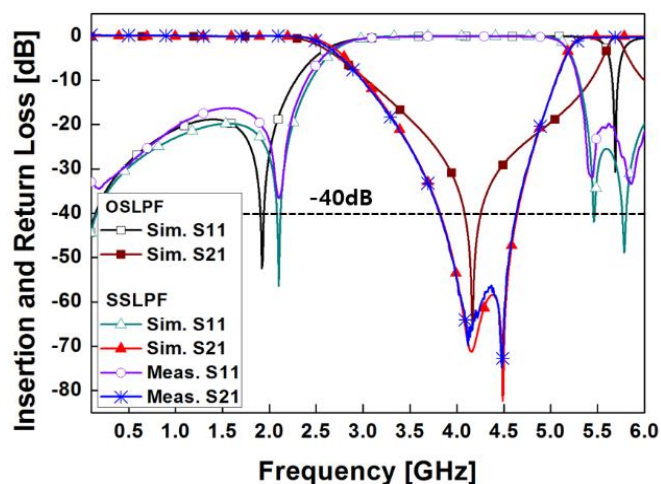

Figure 9. Simulated and measured results of the fabricated SSLPF

The passband return loss and insertion loss were measured to be more than 16.2 dB and less than 0.1 dB, respectively. *Table 1* presents a summary of the characteristics related to attenuation poles.

Table 1. Summary of the results in *figure 9*

Frequency of Attenuation Pole		1st pole [GHz]	2nd pole [GHz]
Structure	OSLPF Sim.	4.17	-
	SSLPF Sim.	4.33	4.48
	Meas.	4.15	4.49

Frequency of -40 dB Atten. Level		From [GHz]	To [GHz]	BW [GHz]
Structure	OSLPF Sim.	4.09	4.26	0.17
	SSLPF Sim.	3.82	4.63	0.81
	Meas.	3.82	4.62	0.80

The relative stopband bandwidth of the SSLPF is observed to be about 4.7 times better than that of the OSLPF but the absolute stopband bandwidth is not very large; nevertheless, it is clear that the proposed structure is advantageous for realizing strong attenuation.

4.2. Fabrication and evaluation of the PSLPF

This LPF was designed as a Chebyshev filter with fc = 2 GHz, N=5, and passband ripple of 0.01 db. The design parameters of the transmission lines for manufacturing were set as Zc1 = 60 Ω, Z_L1 = 100 Ω, Zc = 60 Ω, Zoe = 85 Ω, and Zoo = 75.3 Ω; Φ, θc1, and $θ_L1$ were set as 25.8°, 34.41°, and 40.73°, respectively. In addition, the value of θ calculated by Equation (8) is 11.34°. *Figure 10* shows a photograph of the fabricated PSLPF.
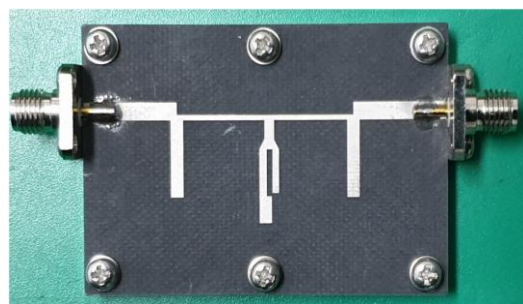

Figure 10. Fabricated PSLPF

Figure 11 shows the EM simulated and measured results of the fabricated PSLPF along with the OSLPF characteristics.
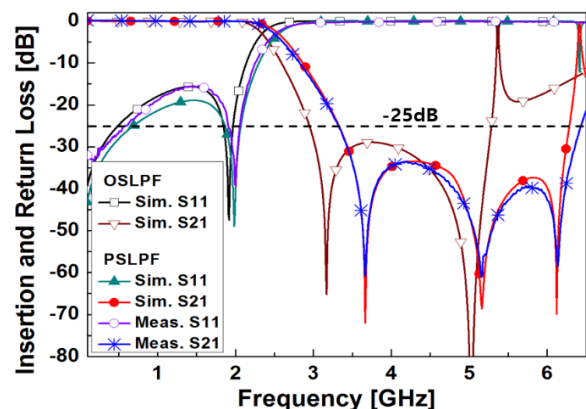

Figure 11. Simulated and measured results of the PSLPF

The passband return loss and insertion loss were measured to be more than 15.4 dB and less than 0.12 dB, respectively. *Table 2* presents a summary of the characteristics related to attenuation poles.

Table 2. Summary of the results in *figure 11*

Frequency of Attenuation Pole			1st pole [GHz]	2nd pole [GHz]	3rd pole [GHz]
Structure	OSLPF	Sim.	3.17	5.13	-
	PSLPF	Sim.	3.66	5.16	6.12
		Meas.	3.67	5.15	6.13
Frequency with -25 dB Level	**Atten.**		From [GHz]	To [GHz]	BW [GHz]
Structure	OSLPF	Sim.	4.09	5.28	2.33
	PSLPF	Sim.	3.82	6.28	2.96
		Meas.	3.82	6.42	3.32

The stopband bandwidth of the PSLPF is approximately 1.4 times better than that of the OSLPF. Although the PSLPF has a relatively small stopband bandwidth ratio compared to the SSLPF, it can suppress the third harmonic adequately. Therefore, if the frequencies of attenuation poles are appropriately arranged based on the length of the spur-line, it may be possible to implement a wider stopband or achieve greater attenuation.

The above results are limited to the fabricated sample SSLPF and OSLPF only and are not general; nevertheless, the above results sufficiently showed us that the two proposed structures were valid, and the design formulas were correctly derived.

5. CONCLUSION

In this study, the SSLPF and PSLPF were designed as spur-lines added to the OSLPF structure in serial and parallel, respectively, to improve the stopband performance. We derived the equations to calculate the design variables for the two structures, and the two LPFs were fabricated according to the design formulas and principles. By comparing the features and analyzing the measured and simulated results of the OSLPF as well as the two proposed LPFs, the validity of the proposed structure and derived equations were demonstrated. From the analysis results, we observed that two proposed LPFs were advantageous for realizing a wide stopband.

It is convinced that an LPF design that simultaneously applies spur-lines to both the serial line and parallel open stub could produce stronger attenuation and wider stopband. In addition, it is believed that the proposed method could be applied similarly to more extended structures than N=5 as considered in this study.

ACKNOWLEDGMENTS

REFERENCES

[1] I. Runsey, M. Picket-May, and P. K. Kelly, "Photonic Bandgap Structure used as Filter in Microstrip Circuits", *IEEE Microwave and Guided Wave Letters*, 1998, *vol. 8, no. 10, 36-338*.

[2] T. Kim and C. Seo, "A Novel Photonic Bandgap Structure for Low-Pass Filter of Wide Stopband", *IEEE Microwave and Guided Wave Letters*, 2002, *vol.10, no. 1, 13-15*.

[3] D. Ahn, J. S. Park, C. S. Kim, J. Kim, Y. Qian, and T. Itoh, "A Design of the Low-Pass Filter the Novel Microstrip Defected Ground Structure", *IEEE Transaction on Microwave Theory and Techniques*, 2001, *vol. 49, no. 1, 86-93*.

[4] J. K. Xiao, Y. F. Zhu, and J. F. Fu, Non-uniform DGS Low Pass Filter with Ultra-wide Stopband, Proceeding of the 9th International Symposium on Antennas, Propagation and EM Theory, Guangzhou, China, Nov. 29-Dec. 2, 2010.

[5] M. H. Kwak, S. K. Han, K. Y. Kang, D. Ahn, J. S. Suh, and S. H. Kim, "Design of High Temperature Superconducting Low-Pass Filter for Broad-Band Harmonic Rejection", *IEEE Transaction on Applied Superconductivity*, 2001, *vol. 11, no. 2, 4023-4026*.

[6] D. H. Lee, Y. W. Lee, J. S. Park, D. Ahn, H. K. Kim, and K. Y. Kang, A Design of The Novel Coupled Line Low-Pass Filter with Attenuation Poles, 1999 IEEE MTT-S International Microwave Symposium Digest, Anaheim, USA, June 13-19, 1999.

[7] H. Liu, T. Bai, R. H. Knoechel, L. Sun, and K. F. Schuenemann, "Ultra-wide Stopband Microstrip Low-Pass Filter for Harmonics Suppression", *Microwave and Optical Technology Letters*, 2007, *vol. 49, no. 9, 2148-2150*.

[8] A. Cassanueva, A. Leon, A. Mediavilla, M. Arias, and N. Amar, Improved Compact Microstrip Low Pass Filter with Novel Distributions of Complementary Split Ring Resonators(CSRRs), 2009 Asia Pacific Microwave Conference, SUNTEC, Singapore, DEC. 2009.

[9] F. C. Chen, R. S. Li, and Q. X. Chu, "Ultra-wide Stopband Low-Pass Filter Using Multiple Transmission Zeros, *IEEE Access*, 2017, *vol. 5, 6437-6443*.

[10] L. Kumar and M. S. parihar, A Wide Stopband Low-Pass Filter with High Roll-off Using Stepped Impedance Resonators, *IEEE Microwave and Wireless Components Letters*, 2018, *vol. 28, no. 5, 404-406*.

[11] H. Liu, T. Bai, R. H. Knoechel, L. Sun, and K. F. Schuenemann, Ultra-wide Stopband Microstrip Low-Pass Filter for Harmonics Suppression, *Microwave and Optical Technology Letters*, 2007, *vol. 49, no. 9, 2148-2150*.

[12] R. N. Bates, Design of Microstrip Spur-line Band-Stop Filter, *IEE Journal on Microwaves, Optics and Acoustics*, 1977, *vol. 1, no. 6, 209-214*.

[13] C. Nguyen, C. Hsieh, and D. W. Ball, Millimeter Wave Printed Circuit Spurline Filters, IEEE MTT-S International Microwave Symposium Digest, Boston, USA, May 31-June 3, 1983.

[14] Ramesh Boddu, Phaninder Vinay, Arindam Deb and Jibendu Sekhar Roy (2022), A Switchable Filtering Antenna Integrated with U-Shaped Resonators for Bluetooth, WLAN & UWB Applications. IJEER 10(4), 1225-1232. DOI: 10.37391/IJEER.100473.